Nano- and Microscale Holes Modulate Cell-Substrate Adhesion, Cytoskeletal Organization, and $-\beta 1$ Integrin Localization in Sv40 Human Corneal Epithelial Cells

Nancy W. Karuri*, Teresa J. Porri, Ralph M. Albrecht, Christopher J. Murphy, and Paul F. Nealey

***Abstract*—Human corneal epithelial cells (HCECs) interface with a basement membrane *in vivo* that possesses complex nanoscale topographic features. We report that synthetic substrates patterned with nano- and microscale holes differentially modulate the proliferation, shape and adhesion of SV40 human corneal epithelial cells (SV40-HCECs) as a function of feature size: 1) Cell proliferation was inhibited on nanoscale features (features size less than 800 nm in pitch) compared to microscale features or planar substrates in identical culture conditions. 2) Cells on nanoscale holes had a stellate morphology compared to those on microscale features that were more evenly spread. 3) Cells adhered more to nanoscale features than to microscale features when exposed to shear stress in a laminar flow chamber. Transmission electron microscopy showed that cells cultured on the 400 nm pitch patterns had longer and more numerous filopodia and retraction fibers than cells cultured on the 1600 nm pitch patterns. Immunogold labeling of $-\beta_1$ integrins revealed that these receptors were localized at the cell periphery and in the aforementioned cytoskeletal elements. Our findings indicate that surface discontinuities and the activation of mechanochemical cell signaling mechanisms may contribute to the observed responses exhibited by SV40-HCECs cultured on nano- and microscale topography.**

***Index Terms*—Adhesion, cornea, cytoskeleton, epithelium, filopodia, holes, morphology, nanoscale, pattern, proliferation, topography.**

I. Introduction

HUMAN CORNEAL epithelial cells in their natural environment lie on a specialized extracellular matrix known as the basement membrane. The basement membrane possesses a complex three-dimensional (3-D) nanoscale topography of pores, bumps, and fibers having typical dimensions of 50–240 nm [1]–[3]. Nanoscale grooves with similar feature dimensions to those found on the basement membrane have been shown to cause alignment and elongation in human corneal epithelial cells (HCECs) [4], [5]. This anisotropic morphological response to the underlying anisotropic groove and ridge patterns is known as contact guidance. Additionally, studies have demonstrated that the size and distribution of focal adhesion plaques in HCECs cultured on grooved substrates is directly influenced by the sizes of the topographic features [5]. In the study by Teixeira et al., focal adhesions were reported to be located on top of the ridges and the width of these structures was dependent on the size of the underlying ridges. HCECs have been shown to be more adherent on nanoscale groove and ridge patterns than on microscale groove and ridge patterns and planar surfaces [4]. The influence of substrate topography on cell-substrate adhesion may translate to an effect on other cell behaviors. For instance, the link between cell-substrate adhesion and cell proliferation is evident in the early stages of oncogenic transformation that are marked by a loss of cell-matrix adhesion during the G1 phase of the cell cycle [6]–[8]. Preliminary evidence from our laboratory has shown that in addition to eliciting an anisotropic morphological response in the overlying HCECs, groove and ridge patterns also influence cell proliferation [9]. Moreover, other studies carried out by our laboratory have demonstrated that substrate topography has the potential to influence a number of cell functions in other cell types: cell shape and the alignment and orientation of focal adhesions and stress fibers in human keratocytes [10] and neuritogenesis in PC12 cells cultured in suboptimal concentrations of nerve growth factor [11].

It has been proposed that the edges of substrate features may facilitate cell-substrate adhesion by acting as nucleation sites for cell-substrate interactions. Studies have shown that condensations of actin, vinculin, and $\alpha_v\beta_1$ gintegrin receptors are localized at the edges of microscale grooves [12], [13]. Clustering of adhesion molecules, such as $-\beta_1$ integrin receptors, induces tyrosine phosphorylation and activates signaling cascades that control cell spreading and cell motility [14], [15]. Previous reports from our laboratory demonstrated, through the use of laminar flow assays, that HCECs on the biological length scale topography, in the form of nanoscale groove and ridge patterns, were more adhesive under a nominal wall shear stress than cells on microscale and planar surfaces [4]. Therefore,

Manuscript received October 9, 2001 ; revised May 30, 2006. This work was supported in part by the U.S. Department of Commerce under Grant BS123456. This work was supported by grants from the National Eye Institute (RO1 EY 012253-01) and NSF MRSEC (DMR-9632527). Facilities at the Center for Nanotechnology at the University of Wisconsin-Madison are supported in part by DARPA/ONR under Grant N00014–97-1–0460. *Asterisk indicates corresponding author.*

*N. W. Karuri is with Department of Molecular Biology, Princeton University, Washington Road, Princeton, NJ 08544, USA (e-mail: nkaruri@molbio.princeton.edu).

T. J. Porri and P. F. Nealey are with Department of Chemical and Biological Engineering, University of Wisconsin, Madison, WI 53706, USA.

R. M. Albrecht is with Department of Animal Science, University of Wisconsin, Madison, WI 53706, USA.

C. J. Murphy is with Department of Surgical Sciences, School of Veterinary Medicine, University of Wisconsin, Madison, WI 53706, USA.

Digital Object Identifier 10.1109/TNB.2006.886570

the difference between cell substrate on nanoscale features compared to that on microscale features may be attributed to enhanced cell-substrate adhesion at surface discontinuities.

For this investigation we used electron beam lithography to fabricate isotropic features composed of cubic arrays of holes and explored their impact on SV40 human corneal epithelial cells (SV40-HCECs) with respect to cell shape, cytoskeletal organization, proliferation, adhesion, and the distribution of $-\beta_1$ integrins. The substrates used in this study contained hole features that had a similar size distribution to groove and ridge topographies used in a previous study [4] and allowed for a comparison of the effect of surface discontinuities on cell-substrate adhesion in two distinct types of topographies: one that elicits an anisotropic cell shape and one that elicits a isotropic cell shape. A parallel plate flow chamber was used as a detachment assay to evaluate the adhesive response of cells. Scanning electron microscopy (SEM) microscopy was used to investigate cell shape and cytoskeletal organization. Transmission electron microscopy (TEM) of immunogold labeled $-\beta_1$ integrins was used investigate the influence of topography on the distribution of these adhesion receptors.

II. Materials and Methods

A. Substrate Preparation

Electron beam lithography was used to fabricate silicon chips containing six 4-mm^2 regions patterned with a cubic array of holes varying in pitch from nano- to microscale. The patterned regions were separated by planar areas that served as controls. The silicon wafers were cleaned and primed with hexamethyldisilazane (Yield Engineering Systems, San Jose, CA) to promote resist adhesion and then spin coated with a 0.36 μm thick UV6 photoresist (Shipley, Malborough, MA) in a resist spinner (Solitec Wafer Processing, Inc., San Jose, CA). A Cambridge Leica EBMF 10.5 electron-beam lithography tool (Center for Nanotechnology, University of Wisconsin, Madison) was used to pattern the photoresist. A postexposure bake was performed on the resist by heating at 130 °C for 60 s on a hot plate. The exposed and baked films were then immersed in developing solution (MF320, Shipley) for 60 s and rinsed in deionized water. Subsequent to resist patterning, a Helicon reactive ion etching tool (Center for Plasma Aided Manufacturing, University of Wisconsin-Madison) was used to create hole features on the silicon surfaces. The remaining resist was removed after etching by immersing the wafers in piranha solution (70% vol H_2SO_4, 30% vol H_2O_2) at 110 °C for 30 min and rinsing repeatedly with deionized water.

A LEO 1530 scanning electron microscope (Leo Electron Microscopy Inc., Thornwood, NY) operating at 5 kV and integrated with image analysis software was used to characterize the substrates. Fig. 1 shows the dimensions of the features on the surfaces measured by SEM and these include the pitch or the lateral center-to-center distance between the holes (p), the diameter of the holes (d), and the spacing between the holes (l). The ratio between the diameter of the holes (d) and the distance between the holes (l) was approximately $1:1$. The pitch was used to define the topographical areas. A total of five silicon chips were used for the laminar flow assays and within each chip the following seven topographical areas were assayed: the 400, 800, 1200, 1600, 2000, and 4000 nm pitch patterns and the planar surface.

B. Cell Culture

Simian virus transformed human corneal epithelial cells (SV40-HCECs, graciously provided by Dr. Araki-Sasaki, Kiniki Central Hospital, Hyogo, Japan), passages 14–39, were grown to 90%–95% confluence in Supplemented Hormonal Epithelial Medium (SHEM; Sigma-Aldrich, Co., St Louis, MO) containing 10% fetal bovine serum (FBS; Sigma-Aldrich). After achieving the desired confluence, the cells were passaged using 0.025% trypsin/0.01% EDTA (Cascade Biologics, Portland, OR) for 10 min at 37 °C and 5% CO_2. Trypsin was then inactivated by the addition of FBS and the cells were centrifuged for 3 min and then resuspended in 10 ml of SHEM medium. The cells were plated on the patterned silicon chips at a density of 90 000 cells/ml in SHEM medium and incubated for 24 h at 37 °C in a 5% CO_2 atmosphere. Previous experiments demonstrated that this period was optimal for the formation of stable cell-substrate interactions on the silicon substrates [4]. The number of cells on the seven topographical areas after the incubation period was determined using fluorescent probes as outlined below.

C. Adhesion Assay

Following incubation the response of SV40-HCECs on the silicon substrates to a nominal wall shear stress was examined. The cells were exposed to a nominal fluid shear stress of 10 Pa for 15 min in a parallel plate flow chamber [4]. Under these conditions, flow can be considered laminar and entrance effects are neglected. The circulating fluid used in the adhesion assay was SHEM medium. At the end of the laminar flow assay, the substrates were prepared for fluorescence microscopy as described below and the number of adherent cells on the different features was determined.

D. Proliferation Assay

Proliferation during the incubation of cells on the silicon substrates was inhibited for some of the experiments. When 90%–95% confluence was reached, mitomycin C was added to the 75 cm^2 flask containing SV40-HCECs at a final concentration of 4 μg/ml. The flasks were incubated at 37 °C with a 5% CO_2 environment for 2 h then rinsed with PBS, trypsinized, resuspended in SHEM media, and plated onto the silicon chips as outlined above (in Section II-B). The number of cells on the various topographies was then determined using fluorescent probes as described below.

E. Fluorescence Microscopy

After incubation the number of cells was determined by fixing the cells and staining for actin filaments and cell nuclei. The fixative used was composed of 4% paraformadlehyde (Electron Microscopy Sciences, Washington, Pa) in phosphate buffered solution (PBS, BioWhitaker, Walkersville, MD) and fixation was carried out at room temperature for 20 min. The cells were then permeabilized in 0.1% triton X-100 (Sigma-Aldrich, Co.) in PBS for 5 min and blocked with 1% bovine serum albumin (BSA, Sigma-Aldrich) in PBS for 20 min. Actin filaments were

labeled by incubating the cells with 5 μg/ml TRITC-phalloidin (Molecular Probes, Inc. Eugene, OR) for 30 min at room temperature and the nucleus was labeled by incubating the cells in 0.3 μM 4', 6-Diamidino-2-phenylindole (DAPI, Molecular Probes, Inc.) for 10 min at room temperature. The substrates were viewed using a Zeiss Axiovert 200 motorized fluorescence microscope (Carl Zeiss Microimaging, Thornwood, NY) and the number of cells on each patterned regions was determined by using a manual blood cell counter. Four areas, each measuring approximately 1 mm^2, were assayed on each patterned area.

F. Transmission and Scanning Electron Microscopy Studies

Scanning electron microscopy imaged both the morphology and cytoskeleton of SV40-HCECs. Preparation of cells for SEM of the cytoskeleton was conducted by adopting published methodologies [16], [17]. We used PHEM buffer as a base for the extraction solution of the cells. PHEM buffer is composed of 60 mM PIPES (Sigma-Aldrich), 25 mM HEPES (Sigma-Aldrich), 10 mM EGTA (Sigma-Aldrich) and 2 mM $MgC1_2$ (Sigma-Aldrich) at a pH of 6.9. The extraction solution was composed of 1% triton X-100 and 4% PEG (MW 40000, Serva, Heidelberg, NY) in PHEM buffer supplemented with 10 μg/ml taxol (Sigma-Aldrich) and 10 μM phalloidin (Sigma-Aldrich). After cell culture the substrates were rinsed with PBS and then incubated with the extraction solution for 3 min. Extraction was performed at room temperature with gentle agitation. Next, the cells were rinsed in 0.1 M cacodylate buffer (Tousimis Corp., Rockville, MD) for $3\times$ 10 min and fixed in 4% glutaraldehyde (Tousimis Corp.) in 0.1 M sodium cacodylate buffer for 2.5 h, and then rinsed again in 0.1 M cacodylate buffer. Once fixed, the cells were incubated in 1% osmium tetroxide (Tousimis Corp.) for one hour and then dehydrated through a series of ethanol concentrations (70, 80, 90, 99, 100 vol%). The final dehydration in ethanol was followed by immersion of the substrates in hexamethyldisilazane (Sigma-Aldrich) for 5 min and then air-drying. The dried cells were coated with 2 nm of platinum and imaged with a LEO 1530 scanning electron microscope operating at an accelerating voltage of 1–5 kV. The projected area of cells on the different topographies was obtained from image analysis of SEM micrographs.

Transmission electron microscopy was used to investigate the localization of immunogold labeled $-\beta_1$ integrins at the basal surface of the cells. Following cell culture, the substrates were rinsed in PBS and then incubated with anti-human $-\beta_1$ integrin antibodies (CD29, Biosource International, Camarillo, CA) in PHEM buffer at a dilution of 1 : 15 for 30 min at room temperature. PHEM buffer was supplemented with 10 μg/ml taxol and 10 μM phalloidin. The cells were then rinsed in the same supplemented buffer then fixed in 4% glutaraledhyde in PBS for 10 min. After rinsing with PBS, anti- specific labeling was blocked with 1% BSA in a buffer containing 20 mM Tris-HCl (Fisher Scientific, Fair Lawn, NJ) at pH 8.0, 0.5 M NaCl (Sigma-Aldrich) and 0.05% Tween 20 (Fisher Scientific). The cells were incubated with the secondary antibody (Donkey Anti-Mouse IgG conjugated to 18 nm gold particles, Jackson Immuno Research Laboratories) at 4 °C for 12 h. The secondary antibody was applied at a dilution of 1 : 10 in 20 mM Tris-HCl at pH 8.0

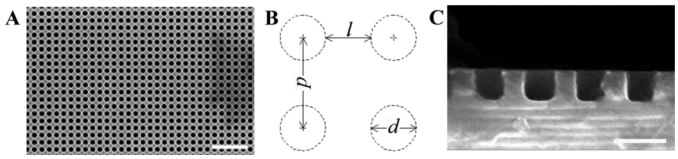

Fig. 1. Substrate characterization. (A) Top down SEM images of the smallest features, the 400 nm pitch patterns (Scale bar = 2 μm). (B) Dimensions evaluated by SEM are pitch (p) or lateral center to center distance, minimum distance between the edges of the holes (l), and the diameter of the holes (d). (C) Cross section image of the 400 nm pitch hole patterns (Scale bar = 400 nm).

supplemented with 0.5 M NaCl, 0.05% Tween 20, and 0.1% BSA. The cells were then repeatedly rinsed with a buffer containing 20 mM Tris-HCl at pH 8.0 supplemented with 0.5 M NaCl, 0.05% Tween 20 and 0.1 BSA. After the final rinse step the cells were first fixed in 4% glutraldehyde in 0.1 M sodium cacodylate buffer for 5 min, then fixed again in 1% osmium tetroxide in 0.1 M sodium cacodylate for 1 h, and finally dehydrated in a graded ethanol series. The cells were infiltrated with a solution containing LR Gold Resin (London Resin Co. Ltd., Berkshire, U.K.) and ethanol for 3 h. The ratio of resin to ethanol in the first infiltration solution was 7 : 3. The first infiltration step was followed by a second in 100% resin, after which the cells were embedded in resin using inverted gel capsules at -27 °C and in UV light. Following embedding, the capsules were separated from the substrates and the resulting resin blocks were cut into 70 nm thick sections (Reichert-Jung Ultracut-E, Leica, Deerfield, IL) and observed by TEM (JEOL 100CX, Peabody, MA).

Negative control experiments were performed to determine the specificity of antibody labeling. Fluorescence microscopy of SV40-HCECs immunostained with isotype IgG2a conjugated to a fluorophore (Sigma-Aldrich) was carried out to determine the affinity of the primary antibody to $-\beta_1$ integrins. The affinity of the secondary antibody to the primary antibody was examined by running parallel TEM studies in which PBS was substituted for the solution containing antibodies against human $-\beta_1$ integrin.

III. Results

Substrate characterization via scanning electron microscopy revealed that the silicon chips contained patterns of cubic arrays of holes with features ranging in size from nanoscale to microscale. Five silicon chips were used for the cell culture assays; each with six 2×2 mm^2 areas patterned with cubic arrays of holes. The pitch dimensions in each chip [p in Fig. 1(a)] were 400, 800, 1200, 1600, 2000, and 4000 nm and the minimum distance between the edges of the holes [l in Fig. 1(b)] was approximately half this value, as shown in Table I(a). The 400, 800, and 1200 nm pitch patterns were separated from each other by a planar area 1.5 mm wide. Approximately 3 mm below the smallest three patterns and having the same separation distance were the 1600, 2000, and 4000 nm pitch patterns. The planar surface separating the two rows of patterns was used as a control for the effect of topography on cell behavior. Fig. 1(a) and 1(c) shows the top down and cross-sectional views of the 400 nm pitch patterns. The values for length of surface discontinuities per unit area (LSD/A) for the 400, 1200, and 4000 nm pitch patterns used in this study and for groove and ridge patterns used in

TABLE I
AVERAGE FEATURE DIMENSIONS OF PATTERNS USED

A

Pitch-p (nm)	Hole diameter-d (nm)
400	255±19
800	455±20
1200	664±26
1600	875±17
2000	1133±30
4000	2222±94

B

Pitch-p (nm)	Length of surface discontinuities per unit area ($\mu m/\mu m^2$)	
	Groove & ridge patterns	*Hole patterns*
400	5.0	5.3
1200	1.7	1.8
4000	0.6	0.5

(A) Lateral dimensions of the hole patterns. (B) Comparison between hole patterns and groove patterns (in [4]) with respect to length of surface discontinuity per unit area available to overlying cells.

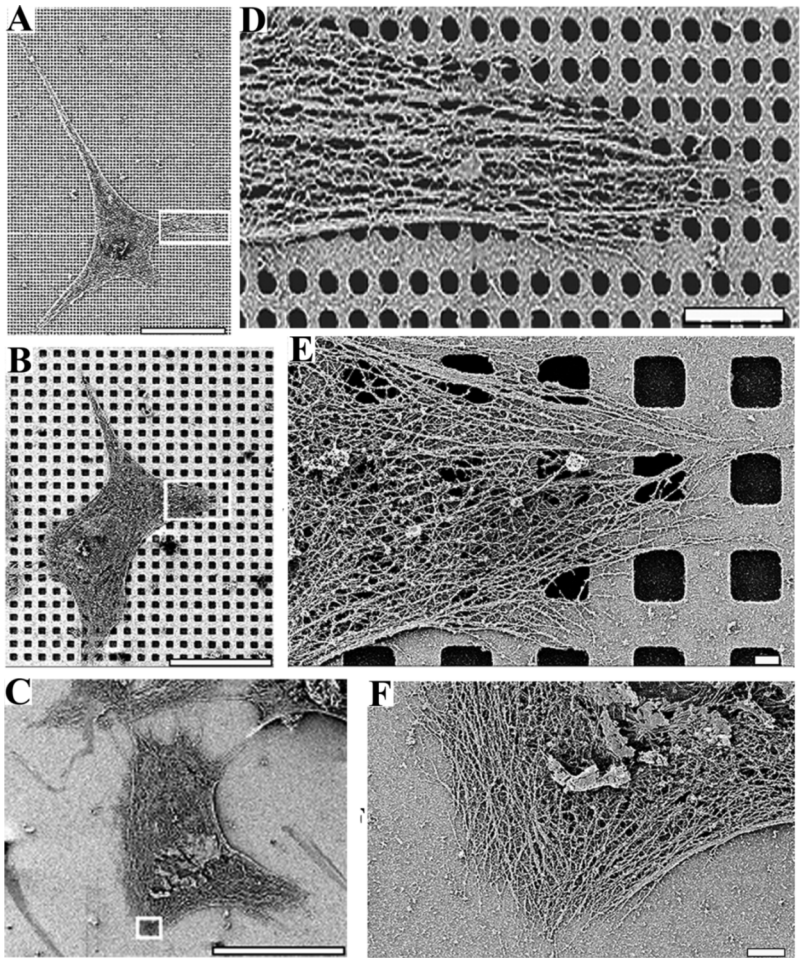

Fig. 2. SEM images of cell morphology and cytoskeleton in cells cultured on hole patterns. (A) 400 nm pitch. (B) 4 μm pitch. (C) Planar surface. (D)-(F) High-magnification representations of the boxed areas in (A)–(C), respectively.

a previous study [4] are shown in Table I(b). The ratio of LSD/A for groove and ridge patterns to the LSD/A for the hole patterns for the 400, 1200, and 4000 nm pitch patterns was 0.94, 0.93, and 1.1 respectively. Hence, for both feature types, the length of surface discontinuities available to the overlying cells was similar. The depth of the holes used in this study was 337 ± 39 nm and was comparable to the depth of the grooves used in the previous study which was 400 ± 150 nm. Therefore, the fabricated silicon chips were used as a basis for investigating the cellular adhesive response to isotropic topographies and how this response compares to that observed for anisotropic topographies.

SEM imaging of the cytoskeleton of extracted SV40-HCECs cultured on the hole patterns demonstrated that cell spreading and cytoskeleton organization was influenced by feature size. Individual SV40-HCECs on the 400 nm pitch hole patterns possessed a morphology that has been described by Dalby and colleagues [18] as stellate [Fig. 2(a)]. Compared to cells on the nanoscale holes, cells on the microscale holes and planar surfaces did not have protrusions extending from the main cells mass and had a more evenly spread morphology [Fig. 2(b) and (c)]. The average projected area of cells on the hole patterns was 998 ± 316 and 1013 ± 189 μm^2 for the 400 nm pitch and the 4000 nm pitch respectively. The cytoskeleton of cells on the nanoscale hole patterns Fig. 2(d) exhibited more bundling than that of cells on the microscale hole patterns, Fig. 2(e), and the planar surfaces, Fig. 2(f). The images in Fig. 2 also show that

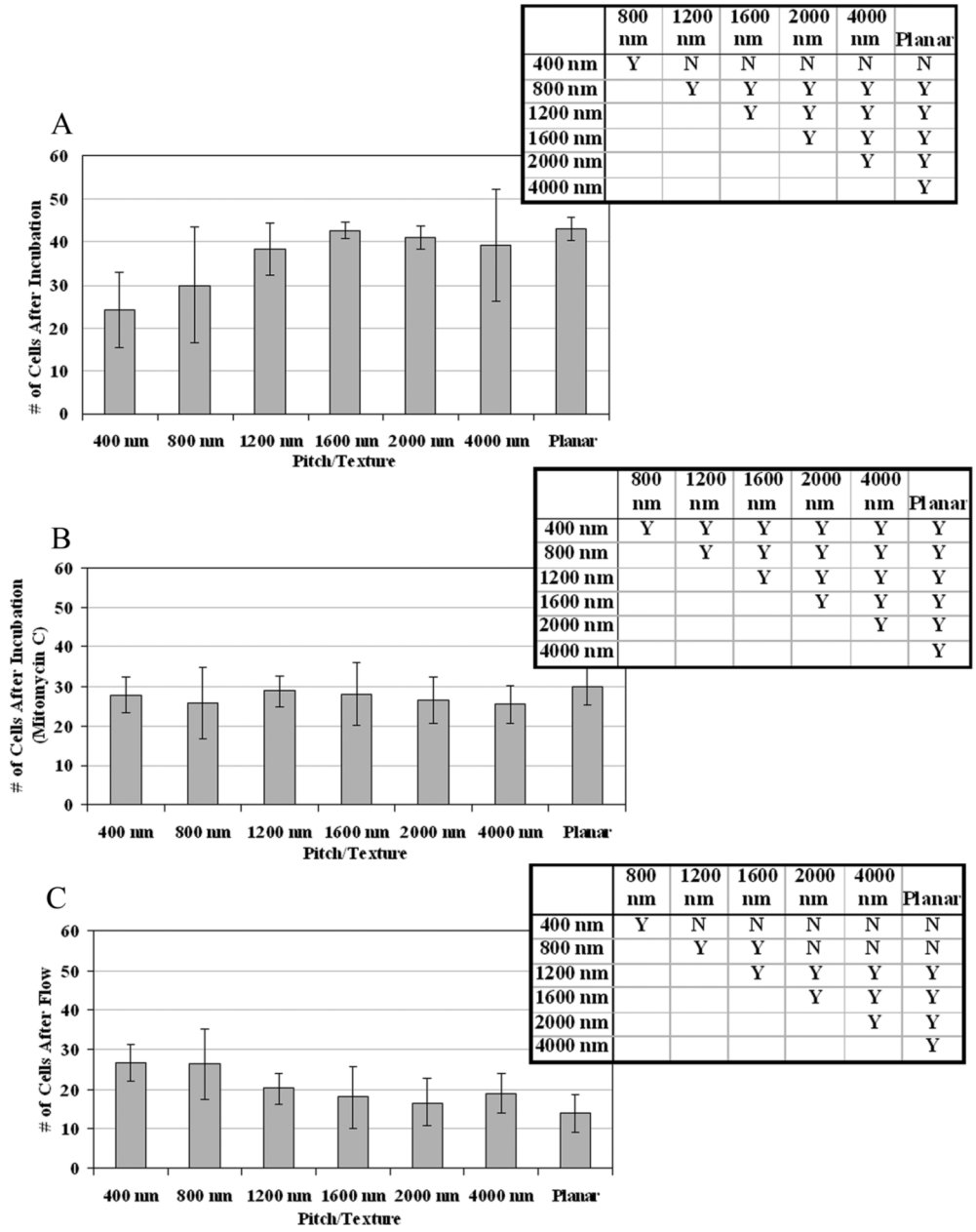

	800 nm	1200 nm	1600 nm	2000 nm	4000 nm	Planar
400 nm	Y	N	N	N	N	N
800 nm		Y	Y	Y	Y	Y
1200 nm			Y	Y	Y	Y
1600 nm				Y	Y	Y
2000 nm					Y	Y
4000 nm						Y

	800 nm	1200 nm	1600 nm	2000 nm	4000 nm	Planar
400 nm	Y	Y	Y	Y	Y	Y
800 nm		Y	Y	Y	Y	Y
1200 nm			Y	Y	Y	Y
1600 nm				Y	Y	Y
2000 nm					Y	Y
4000 nm						Y

	800 nm	1200 nm	1600 nm	2000 nm	4000 nm	Planar
400 nm	Y	N	N	N	N	N
800 nm		Y	Y	N	N	N
1200 nm			Y	Y	Y	Y
1600 nm				Y	Y	Y
2000 nm					Y	Y
4000 nm						Y

Fig. 3. Topography has an effect on proliferation and the response of SV40-HCECs to fluid shear. Number of cells present on the different feature sizes following: (A) a 24-h incubation period (Mean $\pm$ SEM $\times\, t_{95\%,4}$); (B) treatment with Mitomycin C and then a 24-h incubation period (Mean $\pm$ SEM $\times\, t_{95\%,4}$); (C) a 24-h incubation period and then an exposure to fluid shear of 10 Pa for 15 min (Mean $\pm$ SEM $\times\, t_{95\%,16}$). Results for the equality of means test for each figure are shown in the tables next to the figures. A 95% confidence interval was used. The letter Y represents two values that are statistically equal and the letter N represents values that are not. The same passage number and culture conditions were used in (A) and (C).

cells did not spread into the holes but sent out cytoskeleton elements, which were identified as filopodia, to explore the edges of the patterns and reach into the holes. The organization of the cytoskeleton in SV40-HCECs varies from tight bundling on the nanoscale holes to looser networks on the microscale features and cell spreading was consistent with preference of the cell periphery to go around the holes and for the cell body to subsequently span them.

Lower cell numbers were observed on the 400 nm pitch patterns than on the other topographies at the end of the incubation period. A quantitative analysis of this observation is presented in Fig. 3(a). The differences in number of cells on the various topographies after incubation were examined by performing an equality of means test. The results of this test are presented in top right corner of Fig. 3(a) and they confirm that the number of SV40-HCECs on the 400 nm pitch patterns was significantly less than on the patterns with pitch dimensions greater than 800 nm. There were 73% and 74% more cells on the 4000 nm pitch patterns and on the planar surfaces respectively than were on the 400 nm pitch patterns. We examined whether changes in cell numbers on the different feature sizes may have been due to an influence of topography on cell proliferation.

The experiments were repeated using cells that had been incubated in the presence of mitomycin C, a compound that is routinely used to inhibit proliferation in cultured cells. Fig. 3(b) represents the number of cells present after cells were cultured

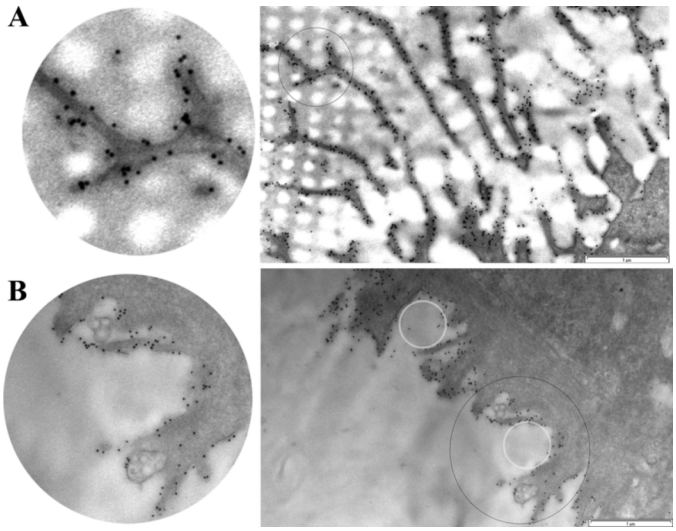

Fig. 4. TEM images of the basal surface of SV40-HCECs cultured on the hole patterns and immunolabeled for $-\beta 1$ integrins. (A) 400 nm pitch and (B) 1600 nm pitch patterns. The white rings in (B) represent positions of the holes. The images on the left show close ups of the images on the right and labeled $-\beta 1$ integrins are marked by the dark spots. Note that filopodia in the cell on the 400 nm pitch patterns are longer and more abundant than filopodia in the cell on the 1600 nm pitch patterns. Scale bar in A = 1 μm and scale bar in B = 1 μm.

in media supplemented with mitomycin C. The results of an equality of means test, shown at the top right hand corner of the figure, demonstrated that the number of SV40-HCECs on the seven different topographies was statistically equivalent. Therefore, reduced cell proliferation on the 400 nm pitch patterns was likely responsible for the lower numbers of cells after incubation.

We observed more adherent SV40-HCECs on the 400 nm pitch patterns than on the other topographies after incubating the cells in an environment where proliferation was not inhibited and exposing them to fluid shear. Fig. 3(c) shows the mean number of cells present after the application of a nominal wall shear stress of 10 Pa for 15 min. The results of an equality of means test demonstrated that cells on the nanoscale features were more resilient to the nominal wall shear stress than cells on topographies having pitch dimensions greater than 800 nm. There were 38% and 33% fewer cells on the 4000 nm pitch and the planar topographies respectively than on the 400 nm pitch patterns. No significant difference was observed in the number of cells on topographies with pitch dimensions of 1200 nm and above. Therefore, there are more adherent SV40-HCECs on the nanoscale features than on the microscale and planar features after the application of a detachment force.

Transmission electron micrographs demonstrated that topography influences cell spreading and the number and extension of filopodia and retraction fibers. Ultrathin sections of the basal undersurface of the cells are shown in Fig. 4. The nanoscale feature sizes are represented by the 400 nm pitch patterns in Fig. 4(a) and the microscale feature sizes are represented by the 1600 nm pitch patterns in Fig. 4(b). The micrographs in Fig. 4 show that lamellipodia developed preferentially on the tops of the surfaces and then extended around edges of the holes. Qualitatively, cells cultured on nanoscale holes exhibited more filopodia and retraction fibers than cells cultured on microscale holes. The interaction of these cytoskeletal elements with the surface was restricted to the tops of the patterns and the edges of the holes. The dark spots in Fig. 4(a) and (b) represent colloidal gold antibody labeling of $-\beta_1$ integrins. A high incidence of $-\beta_1$ integrins was observed both in filopodia and retraction fibers and at the cell periphery. Negative control experiments indicated that both primary and secondary antibody staining was specific (data not shown).

IV. Discussion

In previous studies we demonstrated that the basement membranes of corneal epithelial cells interact with a 3-D nanoscale topography; we created model systems to investigate the effect of topography on cell behavior and established that biological length scale topography leads to enhanced cell-substrate adhesion [1]–[5]. Research into the effect of groove and ridge topography on cell behavior has demonstrated that cells cultured on nanoscale and microscale patterns exhibit contact guidance, a preferential alignment, elongation and migration in the direction of the grooves [4], [5], [10]. Furthermore, laminar flow assays demonstrated that SV40-HCECs cultured on nanoscale grooves were more adhesive under a nominal wall shear stress than cells on microscale grooves and planar surfaces. We attributed this adhesive response to topography to the proposal that surface discontinuities are areas of strong cell-substrate interactions [4]. This study supports our previous findings and demonstrates through the use of isotropic topographies that the size of the features or the number of discontinuities interfaced by cells influences cell-substrate adhesion on patterned substrates. We also show that topographical modulation of cell shape has the potential to influence cell proliferation and cytoskeletal organization.

We used lithographic techniques to create isotropic topography comprising of cubic arrays of hole patterns on silicon chips that had the same size distribution as anisotropic groove and ridge topography used in a previous study [4] and investigated the effect of biological length scale topography on cell behavior. SV40 human corneal epithelial cells cultured on the biological length scale hole topographies exhibited a reduced ability to proliferate than cells cultured on the microscale hole and planar topographies. In a preliminary report, we found that HCECs cultured on 400 nm pitch groove and ridge patterns exhibited decreased proliferation than cells cultured on the microscale feature sizes for incubation periods of five days [9]. Other published studies using incubation periods of two to four days report similar findings; there are fewer cells on nanoscale hole topography compared to planar surfaces [18]–[20].

It may be argued that there are fewer cells initially adhering to the 400 nm surfaces and short-term time experiments are necessary to differentiate this outcome from the effect of topography on cell proliferation. However, fewer cells have been reported on nanoscale groove and ridge patterns than on microscale groove and ridge patterns for culture periods of five days [9] and planar surfaces for culture periods of two to four days [18]–[20]. Therefore, the 24-h period used in this study is relatively short term compared to the aforementioned studies. Furthermore, we have observed in groove and ridge patterns on similar length scales

to the hole surfaces used for this study that there was no significant difference in the number of cells on the different features after incubation periods of 3–12 h [4]. Subsequently, it is likely that the reduced number of cells on nanoscale holes than on microscale holes and planar surfaces is due to a reduced ability of the cells to proliferate on the nanoscale features.

Topography may influence cell proliferation through cell spreading. Cells cultured on nanoscale holes had a stellate structure, similar to that reported for fibroblasts cultured on nanoscale holes [18], while those on the microscale holes were more evenly spread. The link between cell proliferation and cell-substrate adhesion is evident in the ability of integrins to activate mitogenic pathways [21]–[23]. Additionally, micropatterned islands of adhesive proteins that vary cell shape have been shown to influence cell proliferation [24]. While the exact mechanism by which cell spreading influences cell proliferation is not known, the differences in cell proliferation observed on the different topographies may be attributed the influence of topography on cell shape.

The strength of cell-substrate adhesion, measured by a laminar flow assay, was higher in cells cultured on nanoscale hole features than on microscale hole features and planar surfaces. These results are similar to previous results from our laboratory that demonstrated that SV40-HCECs on nanoscale groove and ridge patterns were more adherent than cells on microscale groove and ridge patterns and planar surfaces [4]. Implicit in the interpretation of cell-substrate adhesion data obtained from the laminar flow assay is that a morphological response of cells to the underlying substrate may contribute to the hydrodynamic force experienced by the cells. However, a number of findings in a past study published by our laboratory support the argument that cell shape and deformability do not significantly impact the hydrodynamic force experienced by the cells in a the laminar flow assay used [4]. This is important because there is no difference between the effective force experienced by cells on different feature sizes and on different feature types. We also reported a similar response by the cells to a nominal shear stress when flow was directed parallel and perpendicular to the grooves and therefore parallel and perpendicular to the axis of aligned and elongated cells. Fluid shear detachment assays evaluate a population of cells, and therefore singularities introduced by individual cells are averaged out. Additionally, calculations done using the guidelines of Stroock and colleagues demonstrated that the presence of the patterns on the nominal wall shear stress was negligible [25]. If cell morphology significantly impacts the hydrodynamic force during flow, and hence cell detachment, then it would be expected that the proportion of cells detached would be similar in both nano- and microscale grooves as a similar proportion of cells on the two feature types that exhibits contact guidance. However, we found a statistically smaller proportion of cells detached from the nanoscale groove and ridge patterns than from the microscale groove and ridge patterns and the planar surfaces. Interestingly, hole patterns elicit a different shape response to that observed in groove and ridge patterns but fluid shear detachment assays support our primary finding with the groove and ridge patterns; SV40-HCECs cultured on nanoscale features are more resilient to a nominal fluid shear stress than cells on microscale features and planar surfaces. Therefore, the results obtained from laminar flow assays of cells cultured on groove and ridge patterns and from hole patterns indicate that SV40-HCECs are more adherent on biological length scale topography and supports the proposal shape does not have a significant impact on the nominal wall shear stress in the laminar flow assay.

Higher cell-substrate adhesion on nanoscale hole patterns supports the proposal that surface discontinuities are areas of stable cell-matrix interactions. We found that as the dimensions of the holes increased from nanoscale to microscale, the length of discontinuities per unit area available to overlying cells decreased and so did the ability of the cells to remain attached to the substrate after a nominal wall shear stress. Data obtained from electron micrographs was consistent with a previous study that demonstrated that cell-substrate contact was limited to the top of the patterns [4]. Moreover, cells on both the nanoscale and microscale hole features had a statistically similar average projected area. Therefore, if the effective detachment force experienced by the cells is evaluated as a product of the nominal wall shear stress and the area covered by the cells, then cells on both nano- and microscale features experienced a similar detachment force. Nonetheless, cells on nanoscale hole features were more adhesive than those on the microscale features and planar surfaces. A similar adhesive response was reported in SV40-HCECs on groove and ridge patterns having a similar feature size distribution [4], thereby supporting the proposal that surface discontinuities are areas of enhanced cell-substrate adhesion.

Substrate topography influences the length and abundance of filopodia, their exploration of the surface and cell spreading. Qualitative information from transmission electron micrographs showed that cells cultured on nanoscale holes had more numerous and longer filopodia and retraction fibers than cells on the microscale holes and cells on the planar surface. We also observed that these cytoskeletal elements interacted preferentially with the area between the patterns and curved around the edges of the holes. Both filopodia and retraction fibers consist of bundles of actin fibers and play important roles in cell motility [26]. However, the significance of these cytoskeletal elements in protrusive force generation remains controversial. The typical size of filopodia is 0.1–0.5 μm and their extension length is 5–50 μm. Retraction fibers are smaller in size 40–120 nm in size [27] and exhibit more branching. It is therefore likely that both cystoskeletal elements are present on the nanoscale hole features. Filopodia direct cell spreading as they become stabilized in the direction of cytoskeleton polymerization. Our results showed that lamellipodia formed preferentially in the region between the holes and the cell body subsequently spanned the holes. Furthermore these findings with respect to the response of SV40-HCECs to nanoscale holes are in agreement with other studies using fibroblasts that show more abundant and longer filopodia and retraction fibers than on nanoscale holes than on planar surfaces [18], [28]. The observation that these structures curve around the edges of the patterns also supports the proposal that surface discontinuities may act as favorable guidance cues that direct cell spreading [29]. Furthermore, these findings indicate that the cell through cytoskeletal elements can "read"

the physical environment and hence these elements may play a significant function in mechanosensing.

In addition to sensing topography and guiding cells, filopodia may play an important role in cell-substrate adhesion on nanoscale topography. The adhesive ability of filopodia is supported by the presence of $-\beta_1$ integrins in these structures. Filopodia have been shown to mediate cell-cell adhesion in epithelial cells [30] and have recently been implicated in cell-substrate adhesion [31]. The hole features may supply positive guidance cues for anchorage-dependent cells to attach, leading to enhanced cell attachment at the cell periphery and in filopodia.

V. Conclusion

In this report we have used a dynamic adhesion assay and electron microscopy techniques to demonstrate that nanoscale hole topography enhances the adhesion of SV40-HCECs to the substrate and inhibits cell proliferation. The evidence we have presented from shear detachment of cells on isotropic topographies support the proposal that surface discontinuities are areas of enhanced cell-substrate interactions. The TEM technique used to image the interface between cell and the substrate show that differences exist in cell structure and distribution of adhesion receptors which may contribute to the observed differences in cell-substrate adhesion between nano- and microscale features.

Acknowledgment

The authors would like to thank S. W. Karuri for statistical analysis of the experimental data.

References

[1] G. A. Abrams, E. Bentley, P. F. Nealey, and C. J. Murphy, "Electron microscopy of the canine corneal basement membranes," *Cells Tissues Organs*, vol. 170, pp. 251–257, 2002.

[2] G. A. Abrams, S. L. Goodman, P. F. Nealey, M. Franco, and C. J. Murphy, "Nanoscale topography of the basement membrane underlying the corneal epithelium of the rhesus macaque," *Cell Tissue Res.*, vol. 299, pp. 39–46, 2000.

[3] G. A. Abrams, S. S. Schaus, S. L. Goodman, P. F. Nealey, and C. J. Murphy, "Nanoscale topography of the corneal epithelial basement membrane and descemet's membrane of the human," *Cornea*, vol. 19, pp. 57–64, 2000.

[4] N. W. Karuri, S. Liliensiek, A. I. Teixeira, G. Abrams, S. Campbell, P. F. Nealey, and C. J. Murphy, "Biological length scale topography enhances cell-substratum adhesion of human corneal epithelial cells," *J. Cell Sci.*, vol. 117, pp. 3153–64, 2004.

[5] A. I. Teixeira, G. A. Abrams, P. J. Bertics, C. J. Murphy, and P. F. Nealey, "Epithelial contact guidance on well-defined micro- and nanostructured substrates," *J. Cell Sci.*, vol. 116, pp. 1881–92, 2003.

[6] F. G. Giancotti and E. Ruoslahti, "Integrin signaling," *Science*, vol. 285, pp. 1028–1032, 1999.

[7] T. M. Guadagno, M. Ohtsubo, J. M. Roberts, and R. K. Assoian, "A link between cyclin a expression and adhesion-dependent cell cycle progression," *Science*, vol. 262, pp. 1572–1575, 1993.

[8] E. Ruoslahti, "Fibronectin and its integrin receptors in cancer," *Adv. Cancer Res.*, vol. 76, pp. 1–20, 1999.

[9] C. J. Murphy, P. F. Nealey, and S. F. Campbell, "Substratum topography modulates proliferation of corneal epithelial cells," presented at the Ann. Meeting Association for Research in Vision and Ophthalmology, Fort Lauderdale, FL, 2004.

[10] A. I. Teixeira, P. F. Nealey, and C. J. Murphy, "Responses of human keratocytes to micro- and nanostructured substrates," *J. Biomed. Mater. Res. A*, vol. 71, pp. 369–376, 2004.

[11] J. D. Foley, E. W. Grunwald, P. F. Nealey, and C. J. Murphy, "Cooperative modulation of neuritogenesis by PC12 cells by topography and nerve growth factor," *Biomaterials*, vol. 26, pp. 3639–3644, 2005.

[12] D. M. Brunette, "Fibroblasts on micromachined substrata orient hierarchically to grooves of different dimensions," *Exp. Cell Res.*, vol. 164, pp. 11–26, 1986.

[13] B. Wojciak-Stothard, A. Curtis, W. Monaghan, K. MacDonald, and C. Wilkinson, "Guidance and activation of murine macrophages by nanometric scale topography," *Exp. Cell Res.*, vol. 223, pp. 426–435, 1996.

[14] R. O. Hynes, "Integrins: Versatility, modulation, and signaling in cell adhesion," *Cell*, vol. 69, pp. 11–25, 1992.

[15] R. Pankov, E. Cukierman, K. Clark, K. Matsumoto, C. Hahn, B. Poulin, and K. M. Yamada, "Specific beta1 integrin site selectively regulates Akt/protein kinase B signaling via local activation of protein phosphatase 2A," *J. Biol. Chem.*, vol. 278, pp. 18671–18681, 2003.

[16] M. Schliwa and J. van Blerkom, "Structural interaction of cytoskeletal components," *J. Cell Biol.*, vol. 90, pp. 222–35, 1981.

[17] T. M. Svitkina and G. G. Borisy, "Correlative light and electron microscopy of the cytoskeleton of cultured cells," *Methods Enzymol.*, vol. 298, pp. 570–592, 1998.

[18] M. J. Dalby, M. O. Riehle, H. Johnstone, S. Affrossman, and A. S. Curtis, "Investigating the limits of filopodial sensing: A brief report using sem to image the interaction between 10 nm high nano-topography and fibroblast filopodia," *Cell Biol. Int.*, vol. 28, pp. 229–236, 2004.

[19] A. S. Curtis, N. Gadegaard, M. J. Dalby, M. O. Riehle, C. D. Wilkinson, and G. Aitchison, "Cells react to nanoscale order and symmetry in their surroundings," *IEEE Trans. Nanobiosci.*, vol. 3, no. 1, pp. 61–65, Mar. 2004.

[20] J. O. Gallagher, K. F. McGhee, C. D. Wilkinson, and M. O. Riehle, "Interaction of animal cells with ordered nanotopography," *IEEE Trans. Nanobiosci.*, vol. 1, no. 1, pp. 24–28, Mar. 2002.

[21] R. K. Assoian and X. Zhu, "Cell anchorage and the cytoskeleton as partners in growth factor dependent cell cycle progression," *Curr. Opin. Cell Biol.*, vol. 9, pp. 93–98, 1997.

[22] K. Roovers, G. Davey, X. Zhu, M. E. Bottazzi, and R. K. Assoian, "Alpha5beta1 integrin controls cyclin D1 expression by sustaining mitogen-activated protein kinase activity in growth factor-treated cells," *Mol. Biol. Cell*, vol. 10, pp. 3197–3204, 1999.

[23] X. Zhu and R. K. Assoian, "Integrin-dependent activation of MAP kinase: A link to shape-dependent cell proliferation," *Mol. Biol. Cell*, vol. 6, pp. 273–282, 1995.

[24] S. Huang, C. S. Chen, and D. E. Ingber, "Control of cyclin D1, p27(Kip1), and cell cycle progression in human capillary endothelial cells by cell shape and cytoskeletal tension," *Mol. Biol. Cell*, vol. 9, pp. 3179–3193, 1998.

[25] A. D. Stroock, S. K. Dertinger, G. M. Whitesides, and A. Ajdari, "Patterning flows using grooved surfaces," *Anal. Chem.*, vol. 74, pp. 5306–5312, 2002.

[26] T. J. Mitchison and L. P. Cramer, "Actin-based cell motility and cell locomotion," *Cell*, vol. 84, pp. 371–379, 1996.

[27] L. Cramer and T. J. Mitchison, "Moving and stationary actin filaments are involved in spreading of postmitotic PtK2 cells," *J. Cell Biol.*, vol. 122, pp. 833–843, 1993.

[28] M. J. Dalby, M. O. Riehle, H. J. Johnstone, S. Affrossman, and A. S. Curtis, "Polymer-demixed nanotopography: Control of fibroblast spreading and proliferation," *Tissue Eng.*, vol. 8, pp. 1099–1108, 2002.

[29] C. Oakley and D. M. Brunette, "The sequence of alignment of microtubules, focal contacts and actin filaments in fibroblasts spreading on smooth and grooved titanium substrata," *J. Cell Sci.*, vol. 106, pt. 1, pp. 343–354, 1993.

[30] W. Wood and P. Martin, "Structures in focus-filopodia," *Int. J. Biochem. Cell Biol.*, vol. 34, pp. 726–730, 2002.

[31] X. Zhu, J. Chen, L. Scheideler, T. Altebaeumer, J. Geis-Gerstorfer, and D. Kern, "Cellular reactions of osteoblasts to micron- and submicron-scale porous structures of titanium surfaces," *Cells Tissues Organs*, vol. 178, pp. 13–22, 2004.

[32] C. S. Chen, M. Mrksich, S. Huang, G. M. Whitesides, and D. E. Ingber, "Geometric control of cell life and death," *Science*, vol. 276, pp. 1425–1428, 1997.

[33] K. K. Parker, A. L. Brock, C. Brangwynne, R. J. Mannix, N. Wang, E. Ostuni, N. A. Geisse, J. C. Adams, G. M. Whitesides, and D. E. Ingber, "Directional control of lamellipodia extension by constraining cell shape and orienting cell tractional forces," *FASEB J.*, vol. 16, pp. 1195–1204, 2002.

Authors' photographs and biographies not available at the time of publication.